A Novel Transformer Winding Design Strategy for Efficiency Improvement and Harmonic Suppression in Industrial Power System

Qianyi Liu, Fang Liu, Yi Yang, Yanjian Peng, Kang-Zhi Liu, and Ao Wang

***Abstract*—Large-power industrial power supply system is generally recognized as high energy-consuming, while the rectifier transformer is the key for efficiency promotion. This article proposes a novel transformer winding design strategy with the aims of harmonic elimination and loss reduction. By means of the innovative impedance matching design, the harmonic magnetic potential self-balance between the secondary windings is realized for harmonic suppression. Considering the impedance constraint and the margin of structural parameters, the method of resistance loss reduction is explored for the proposed transformer by optimizing the dimension parameters. The transformer-filter combination is first modeled to reveal the filtering principle and obtain the impedance precondition. Then, the transformer efficiency is optimized within the constraints. At last, the transformer prototype together with the power supply system is tested. The experimental results show that the transformer efficiency can be improved by 0.81%, and the current total harmonic distortion at primary side is dropped by 50%.**

***Index Terms*—Power quality, industrial power system, rectifier transformer, efficiency improvement.**

Received: December 12, 2023
Accepted: May 1, 2024
Published Online: November 1, 2024

Qianyi Liu, Fang Liu (corresponding author), and Yi Yang are with the School of Automation, Central South University, Changsha 410083, China (e-mail: liu7y@foxmail.com; csuliufang@csu.edu.cn; yy.one@qq.com).

Yanjian Peng is the College of Electrical and Information Engineering, Hunan University, Changsha 410082, China (e-mail: yjpeng@csust.edu.cn).

Kang-Zhi Liu is with the Department of Electrical and Electronic Engineering, Chiba University, Chiba 263-8522, Japan (e-mail: kzliu@faculty.chiba-u.jp).

Ao Wang is with Jiangsu Province Engineering Research Center of High-level Energy and Power Equipment, Changzhou University, Changzhou 213164, China (e-mail: wanga@cczu.edu.cn).

DOI: 10.23919/PCMP.2023.000302

I. Introduction

Large-power rectifier system is widely applied in the electrolytic chemical industry, while such industrial power supply system is characterized with high current, which is typically up to thousands or even ten thousands of amperes [1]–[5]. The well-proven diode or thyristor has reliable and cost-effective performance, in turn, its nonlinearity leads to considerable harmonic issues on the industrial power supply system. The harmonic current determines the increasing losses of the power apparatus.

The authors made an on-site efficiency test of the industrial power supply system in an electrolytic manganese factory. Its power supply system consists of 5 rectifier units, and the transformer capacity for each unit is 6 MVA. The current at AC side of rectifier is as fairly high as 5 kA with serious harmonic distortion. Table I and Fig. 1 show the measuring results of the corresponding rectifier units. It can be concluded that the low rectifier transformer efficiency becomes the key factor affecting the whole operating efficiency (η). The average transformer efficiency for the five units is only 95.26%. The excessive loss may lead to hot spots on the core surfaces of the rectifier transformer and result in deterioration of the core insulation and degradation of the insulating oil [6]–[8]. Also, the rectifier transformer always requires additional capacity when operating in harmonic environment, which causes unnecessary waste [9]. It is of significance to implement harmonic suppression and improve transformer efficiency in the high energy-consuming industry.

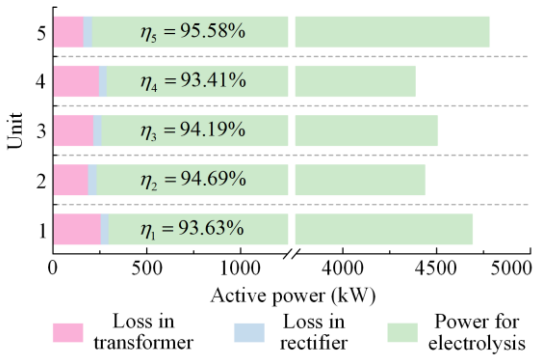

Fig. 1. Composition of the loss in the rectifier units.

TABLE I
MEASURED EFFICIENCY OF A RECTIFIER SYSTEM

Unit	Transformer efficiency (%)	Rectifier efficiency (%)	Unit efficiency (%)
#1	94.52	99.05	93.63
#2	95.72	98.92	94.69
#3	95.17	98.97	94.19
#4	94.35	99.00	93.41
#5	96.56	98.98	95.58

In effect, the transformer losses can be classified as [10].

1) The I^2R loss (R refers to the winding resistance), which is mainly influenced by the flowing current;

2) The winding eddy current loss, which is proportional to the square of the frequency (related to the harmonic currents) and may cause abnormal winding temperature rise;

3) Other stray losses in the core, clamps, and other structural parts.

Therefore, the low-loss improvement can be realized by reducing the winding resistance or eliminating the undesirable current [11]–[18]. Reference [11] adopts the amorphous wound core combined with a grain-oriented silicon steel stacked core to realize the lower iron loss in a larger capacity transformer. A novel transformer featured with low noise and low loss properties is developed by the application of the grooved silicon steel [12]. As for harmonic suppression, reference [13] utilizes the existing tertiary winding of the transformer to construct a tuned low-impedance path for the harmonic currents, but its performance is limited by the winding impedance. A winding tap injection method is proposed in [14], which can make full use of the spare capacity of the transformer and obtain a flexible connection voltage for the compensator. Moreover, the round-shaped transformer proposed in [15] and [16] is effective to reduce harmonic content with potential advantages in weight and dimension. Based on the principle of harmonic magnetic potential self-balance, references [17] and [18] propose the inductive filtering method to solve the difficulty of harmonic suppression in high-current application.

However, few literatures involve the optimization of structural dimension to improve transformer efficiency, especially for the inductive filtering transformer with special requirement of impedance-matching. In light of this, the article proposes a novel winding design strategy for the multi-winding rectifier transformer applied in the 12-pluse rectifier system, with the purpose of harmonic suppression and loss reduction. Its suitable application is the large-power rectifier system with high current. This work tries to solve the following questions.

1) What is the filtering principle of the special transformer-filter combination?

2) How to get the precondition of low-loss design for the multi-winding transformer?

3) How to determine the design margin of the transformer?

4) Considering the constraint of precondition, how to realize the efficiency improvement?

This paper is organized as follows. The description of the transformer together with the industrial power supply system is introduced in Section II. In Section III, the transformer model is established. In Section IV, the efficiency optimization is explored. Moreover, Section V gives the test results. At last, Section VI is the conclusion.

II. DESCRIPTION

A. Transformer

The structure model of the multi-winding rectifier transformer is shown in Fig. 2. It can be obviously known that it is a three-phase four-winding transformer. The windings from inside to outside are arranged as load winding (W3), load winding (W4), filtering winding (W2), and primary winding (W1). According to the basic principle for implementing inductive harmonic suppression [15], the equivalent impedance of W2 should satisfy zero-impedance design, so that the magnetic potential balance can be realized at the harmonic domain. The special impedance design requires the middle arrangement of W2.

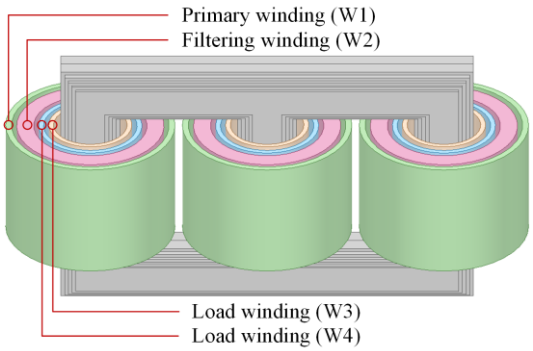

Fig. 2. Model of the multi-winding rectifier transformer.

B. Power Supply System

An industrial power supply system based on the multi-winding rectifier transformer is constructed as shown in Fig. 3. The primary winding is connected to the power grid with star wiring, while the two load windings adopt Y-connection and Δ-connection to form the phase difference of 30°. The filtering winding directly accesses to the filter set. The low-loss improvement of the industrial power supply system is implemented in the following two ways.

1) By means of the inductive filtering method, the flowing path of the undesired currents in the transformer can be considerably shortened, while the electromagnetic environment inside the transformer is im-

proved and the negative effects of harmful components on the transformer are also mitigated.

2) By means of the proposed structural optimization method, the transformer loss is further reduced. The optimal transformer efficiency can be searched and determined in the acceptable range of approximative zero-impedance.

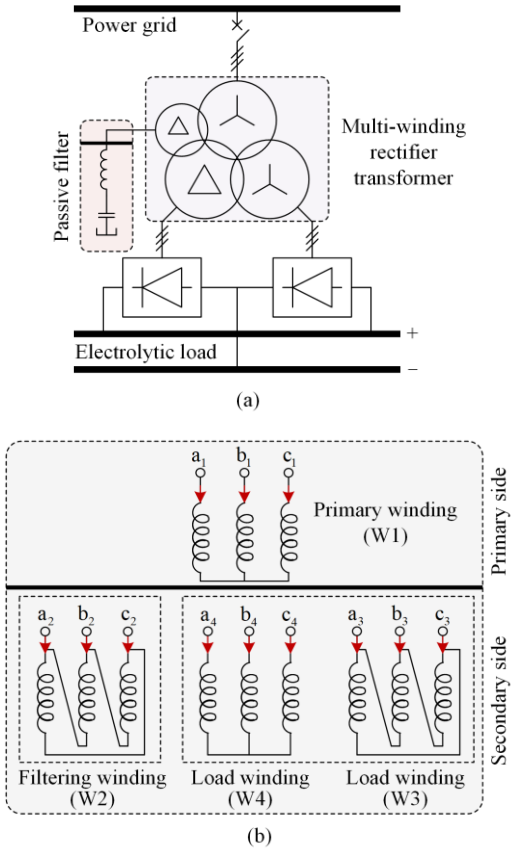

Fig. 3. Proposed industrial supply system. (a) Topology. (b) Wiring scheme.

III. Modelling

A. Precondition

According to the circuit model shown in Fig. 4, the voltage of each transformer winding can be expressed as (1).

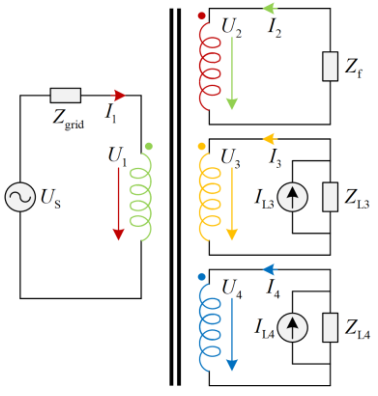

Fig. 4. Circuit model of the industrial power supply system.

$$\begin{cases} U_1 = -E + I_1(\mathrm{j}\omega L_1 + R_1) + I_2\mathrm{j}\omega M_{12} + \\ \qquad I_3\mathrm{j}\omega M_{13} + I_4\mathrm{j}\omega M_{14} \\ U_2 = -E + I_1\mathrm{j}\omega M_{21} + I_2(\mathrm{j}\omega L_2 + R_2) + \\ \qquad I_3\mathrm{j}\omega M_{23} + I_4\mathrm{j}\omega M_{24} \\ U_3 = -E + I_1\mathrm{j}\omega M_{31} + I_2\mathrm{j}\omega M_{32} + \\ \qquad I_3(\mathrm{j}\omega L_3 + R_3) + I_4\mathrm{j}\omega M_{34} \\ U_4 = -E + I_1\mathrm{j}\omega M_{41} + I_2\mathrm{j}\omega M_{42} + \\ \qquad I_3\mathrm{j}\omega M_{43} + I_4(\mathrm{j}\omega L_4 + R_4) \end{cases} \tag{1}$$

where $I_x(x=1,2,3,4)$, which has been converted to primary side, is the current flowing through the winding; $U_x(x=1,2,3,4)$ is the voltage across the corresponding winding; E is the induced electromotive force; $L_1 - L_4$ and $R_1 - R_4$ are the leakage self-inductance and internal resistance of each winding; ω is the circular frequency; M_{xy} is the mutual inductance between winding x and winding $y\,(x,y=1,2,3,4)$, and $M_{xy} = M_{yx}$.

Based on the relationship of ampere-turns balance and the basic principle of circuit, the following equations hold.

$$I_1 + I_2 + I_3 + I_4 = 0 \tag{2}$$

$$\begin{cases} U_1 = U_S - I_1 Z_{grid} \\ U_2 = -I_2 Z_f \\ I_3 = I_{L3} - \dfrac{U_3}{Z_{L3}} \\ I_4 = I_{L4} - \dfrac{U_4}{Z_{L4}} \end{cases} \tag{3}$$

where U_S is the grid voltage included harmonic components; Z_{grid} is grid impedance; Z_f is the equivalent impedance of passive filter; I_{L3} and Z_{L3}, I_{L4} and Z_{L4} are the Norton equivalent of the power load.

Combined with (1) and (2), we can obtain the voltage relationship between each winding as shown in (4), where the short-circuit resistance between winding x and winding y is defined as $R_{kxy} = R_x + R_y$, the short-circuit inductance is $X_{kxy} = \omega(L_x + L_y - M_{xy} - M_{yx})$; the short-circuit impedance is thus expressed as $Z_{kxy} = R_{kxy} + \mathrm{j}X_{kxy}$; Z_{xyz} is the equivalent leakage impedance, $Z_{xyz} = (Z_{kxy} + Z_{kxz} - Z_{kyz})/2$, and $Z_{kxy} = Z_{kyx}\,(x,y,z=1,2,3,4)$.

Combined with (2), (3) and (4.2), we can obtain the grid-side current expressed by the current source or voltage source, as shown in (5). To realize the harmonic-free environment at primary side, the numerator of (5) should be zero.

$$\begin{cases} U_2-U_1=I_2\underbrace{[(R_1+R_2)+\mathrm{j}\omega(L_1+L_2-M_{21}-M_{12})]}_{Z_{k12}}+ \\ \quad I_3\underbrace{[R_1+\mathrm{j}\omega(L_1+M_{23}-M_{21}-M_{13})]}_{Z_{123}}+ \\ \quad I_4\underbrace{[R_1+\mathrm{j}\omega(L_1+M_{24}-M_{21}-M_{14})]}_{Z_{124}} \\ U_3-U_1=I_2\underbrace{[R_1+\mathrm{j}\omega(L_1+M_{32}-M_{31}-M_{12})]}_{Z_{132}}+ \\ \quad I_3\underbrace{[(R_1+R_3)+\mathrm{j}\omega(L_1+L_3-M_{31}-M_{13})]}_{Z_{k13}}+ \\ \quad I_4\underbrace{[R_1+\mathrm{j}\omega(L_1+M_{34}-M_{31}-M_{14})]}_{Z_{134}} \\ U_4-U_1=I_2\underbrace{[R_1+\mathrm{j}\omega(L_1+M_{42}-M_{41}-M_{12})]}_{Z_{142}}+ \\ \quad I_3\underbrace{[R_1+\mathrm{j}\omega(L_1+M_{43}-M_{41}-M_{13})]}_{Z_{143}}+ \\ \quad I_4\underbrace{[(R_1+R_4)+\mathrm{j}\omega(L_1+L_4-M_{41}-M_{14})]}_{Z_{k14}} \end{cases} \tag{4.1}$$

$$\begin{cases} U_1-U_3=I_1\underbrace{[(R_3+R_1)+\mathrm{j}\omega(L_3+L_1-M_{31}-M_{13})]}_{Z_{k31}}+ \\ \quad I_2\underbrace{[R_3+\mathrm{j}\omega(L_3+M_{12}-M_{32}-M_{13})]}_{Z_{312}}+ \\ \quad I_4\underbrace{[R_3+\mathrm{j}\omega(L_3+M_{14}-M_{34}-M_{13})]}_{Z_{314}} \\ U_2-U_3=I_1\underbrace{[R_3+\mathrm{j}\omega(L_3+M_{21}-M_{31}-M_{23})]}_{Z_{321}}+ \\ \quad I_2\underbrace{[(R_3+R_2)+\mathrm{j}\omega(L_3+L_2-M_{32}-M_{23})]}_{Z_{k32}}+ \\ \quad I_4\underbrace{[R_3+\mathrm{j}\omega(L_3+M_{34}-M_{34}-M_{23})]}_{Z_{324}} \\ U_4-U_3=I_1\underbrace{[R_3+\mathrm{j}\omega(L_3+M_{41}-M_{31}-M_{43})]}_{Z_{341}}+ \\ \quad I_2\underbrace{[R_3+\mathrm{j}\omega(L_3+M_{42}-M_{32}-M_{43})]}_{Z_{342}}+ \\ \quad I_4\underbrace{[(R_3+R_4)+\mathrm{j}\omega(L_3+L_4-M_{34}-M_{43})]}_{Z_{k34}} \end{cases} \tag{4.3}$$

$$\begin{cases} U_1-U_2=I_1\underbrace{[(R_2+R_1)+\mathrm{j}\omega(L_2+L_1-M_{21}-M_{12})]}_{Z_{k21}}+ \\ \quad I_3\underbrace{[R_2+\mathrm{j}\omega(L_2+M_{13}-M_{23}-M_{12})]}_{Z_{213}}+ \\ \quad I_4\underbrace{[R_2+\mathrm{j}\omega(L_2+M_{14}-M_{24}-M_{12})]}_{Z_{214}} \\ U_3-U_2=I_1\underbrace{[R_2+\mathrm{j}\omega(L_2+M_{31}-M_{21}-M_{32})]}_{Z_{231}}+ \\ \quad I_3\underbrace{[(R_2+R_3)+\mathrm{j}\omega(L_2+L_3-M_{23}-M_{32})]}_{Z_{k23}}+ \\ \quad I_4\underbrace{[R_2+\mathrm{j}\omega(L_2+M_{34}-M_{24}-M_{32})]}_{Z_{234}} \\ U_4-U_2=I_1\underbrace{[R_2+\mathrm{j}\omega(L_1+M_{41}-M_{21}-M_{42})]}_{Z_{241}}+ \\ \quad I_3\underbrace{[R_2+\mathrm{j}\omega(L_2+M_{43}-M_{23}-M_{42})]}_{Z_{243}}+ \\ \quad I_4\underbrace{[(R_2+R_4)+\mathrm{j}\omega(L_2+L_4-M_{24}-M_{42})]}_{Z_{k24}} \end{cases} \tag{4.2}$$

$$\begin{cases} U_1-U_4=I_1\underbrace{[(R_4+R_1)+\mathrm{j}\omega(L_4+L_1-M_{41}-M_{14})]}_{Z_{k41}}+ \\ \quad I_2\underbrace{[R_4+\mathrm{j}\omega(L_4+M_{12}-M_{42}-M_{14})]}_{Z_{412}}+ \\ \quad I_3\underbrace{[R_4+\mathrm{j}\omega(L_4+M_{13}-M_{43}-M_{14})]}_{Z_{413}} \\ U_2-U_4=I_1\underbrace{[R_4+\mathrm{j}\omega(L_4+M_{21}-M_{41}-M_{24})]}_{Z_{421}}+ \\ \quad I_2\underbrace{[(R_4+R_2)+\mathrm{j}\omega(L_4+L_2-M_{42}-M_{24})]}_{Z_{k42}}+ \\ \quad I_3\underbrace{[R_4+\mathrm{j}\omega(L_4+M_{23}-M_{43}-M_{24})]}_{Z_{423}} \\ U_3-U_4=I_1\underbrace{[R_4+\mathrm{j}\omega(L_4+M_{31}-M_{41}-M_{34})]}_{Z_{431}}+ \\ \quad I_2\underbrace{[R_4+\mathrm{j}\omega(L_4+M_{32}-M_{42}-M_{34})]}_{Z_{432}}+ \\ \quad I_3\underbrace{[(R_4+R_3)+\mathrm{j}\omega(L_4+L_3-M_{43}-M_{34})]}_{Z_{k43}} \end{cases} \tag{4.4}$$

$$I_1=\frac{\left\{\begin{array}{l}[Z_{k23}Z_{k24}-Z_{234}^2+Z_{L3}Z_{L4}+Z_{L3}Z_{k24}+Z_{L4}Z_{k23}+Z_f(Z_{L3}+Z_{L4}+Z_{k23}+Z_{k24}-2Z_{234})]U_S+ \\ [Z_{L3}Z_{214}Z_{234}-Z_{213}Z_{L3}(Z_{L4}+Z_{k24})+Z_fZ_{L3}(Z_{214}+Z_{234}-Z_{213}-Z_{L4}-Z_{k24})]I_{L3}+ \\ [Z_{L4}Z_{213}Z_{234}-Z_{214}Z_{L4}(Z_{L3}+Z_{k23})+Z_fZ_{L4}(Z_{213}+Z_{234}-Z_{214}-Z_{L3}-Z_{k23})]I_{L4}\end{array}\right\}}{\left\{\begin{array}{l}(Z_{k21}+Z_{grid})(Z_{k23}Z_{k24}-Z_{234}^2+Z_{L3}Z_{L4}+Z_{L3}Z_{k24}+Z_{L4}Z_{k23})+2Z_{213}Z_{214}Z_{234}-Z_{213}^2(Z_{k24}+Z_{L4})-Z_{214}^2(Z_{k23}+Z_{L3})+ \\ Z_f[(Z_{k21}+Z_{grid})(Z_{L3}+Z_{L4}+Z_{k23}+Z_{k24}-2Z_{234})+Z_{k23}Z_{k24}+Z_{L3}Z_{L4}-Z_{213}^2-Z_{214}^2-Z_{234}^2+ \\ 2Z_{213}Z_{214}+2Z_{213}Z_{234}+2Z_{214}Z_{234}-2Z_{213}Z_{L4}-2Z_{214}Z_{L3}-2Z_{213}Z_{k24}-2Z_{214}Z_{k23}+Z_{L3}Z_{k24}+Z_{L4}Z_{k23}]\end{array}\right\}} \tag{5}$$

For current source part at harmonic domain, there are:

1) The equivalent impedance of passive filter should be zero at the tuned harmonic frequency, i.e., $Z_f=0$.

2) The rest parts of $Z_{L3}[Z_{214}Z_{234}-Z_{213}(Z_{L4}+Z_{k24})]$ and $Z_{L4}[Z_{213}Z_{234}-Z_{214}(Z_{L3}+Z_{k23})]$ should be zero, and Z_{L3} and Z_{L4} are unequal to zero. As a result, it is required that $Z_{213}=Z_{214}=0$.

The above impedance constraints together constitute the inductive filtering preconditions.

For voltage source part at harmonic domain, the equation (5) can be simplified as follows using the deduced impedance constraints.

$$I_1=\frac{U_S}{Z_{k12}+Z_{grid}} \tag{6}$$

It can be found that a large value of Z_{k12} is beneficial to suppress the harmonics from the upstream.

B. Simplified Circuit

Furthermore, based on the obtained (4), the impedance relationship between each winding can be deduced as follows:

$$I_x = \frac{U_x - U_y}{Z_{xy}} + \frac{U_x - U_z}{Z_{xz}} + \frac{U_x - U_w}{Z_{xw}} \tag{7}$$

where the expressions of Z_{xy}, Z_{xz} and Z_{xw} ($x, y, z, w = 1, 2, 3, 4$) can be referred to (8).

$$\begin{cases}
Z_{12} = Z_{21} = \dfrac{Z_{k21}(Z_{k23}Z_{k24} - Z_{234}^2) + Z_{213}(Z_{214}Z_{234} - Z_{213}Z_{k24}) + Z_{214}(Z_{213}Z_{234} - Z_{214}Z_{k23})}{(Z_{k23}Z_{k24} - Z_{234}^2) + (Z_{234}Z_{214} - Z_{214}Z_{k23}) + (Z_{234}Z_{213} - Z_{213}Z_{k24})} \\
Z_{13} = Z_{31} = \dfrac{Z_{k21}(Z_{k23}Z_{k24} - Z_{234}^2) + Z_{213}(Z_{214}Z_{234} - Z_{213}Z_{k24}) + Z_{214}(Z_{213}Z_{234} - Z_{214}Z_{k23})}{(Z_{k12}Z_{k14} - Z_{124}^2) + (Z_{124}Z_{134} - Z_{134}Z_{k12}) + (Z_{124}Z_{123} - Z_{123}Z_{k14})} \\
Z_{14} = Z_{41} = \dfrac{Z_{k21}(Z_{k23}Z_{k24} - Z_{234}^2) + Z_{213}(Z_{214}Z_{234} - Z_{213}Z_{k24}) + Z_{214}(Z_{213}Z_{234} - Z_{214}Z_{k23})}{(Z_{k12}Z_{k13} - Z_{123}^2) + (Z_{123}Z_{134} - Z_{134}Z_{k12}) + (Z_{123}Z_{124} - Z_{124}Z_{k13})} \\
Z_{23} = Z_{32} = \dfrac{Z_{k21}(Z_{k23}Z_{k24} - Z_{234}^2) + Z_{213}(Z_{214}Z_{234} - Z_{213}Z_{k24}) + Z_{214}(Z_{213}Z_{234} - Z_{214}Z_{k23})}{(Z_{k21}Z_{k24} - Z_{214}^2) + (Z_{214}Z_{234} - Z_{234}Z_{k21}) + (Z_{214}Z_{213} - Z_{213}Z_{k24})} \\
Z_{24} = Z_{42} = \dfrac{Z_{k21}(Z_{k23}Z_{k24} - Z_{234}^2) + Z_{213}(Z_{214}Z_{234} - Z_{213}Z_{k24}) + Z_{214}(Z_{213}Z_{234} - Z_{214}Z_{k23})}{(Z_{k21}Z_{k23} - Z_{213}^2) + (Z_{213}Z_{234} - Z_{234}Z_{k21}) + (Z_{213}Z_{214} - Z_{214}Z_{k23})} \\
Z_{34} = Z_{43} = \dfrac{Z_{k21}(Z_{k23}Z_{k24} - Z_{234}^2) + Z_{213}(Z_{214}Z_{234} - Z_{213}Z_{k24}) + Z_{214}(Z_{213}Z_{234} - Z_{214}Z_{k23})}{(Z_{k32}Z_{k31} - Z_{312}^2) + (Z_{312}Z_{314} - Z_{314}Z_{k32}) + (Z_{312}Z_{324} - Z_{324}Z_{k31})}
\end{cases} \tag{8}$$

According to (7), we can obtain the equivalent circuit of the four-winding transformer as shown in Fig. 5, which is simplified to a quadrilateral circuit.

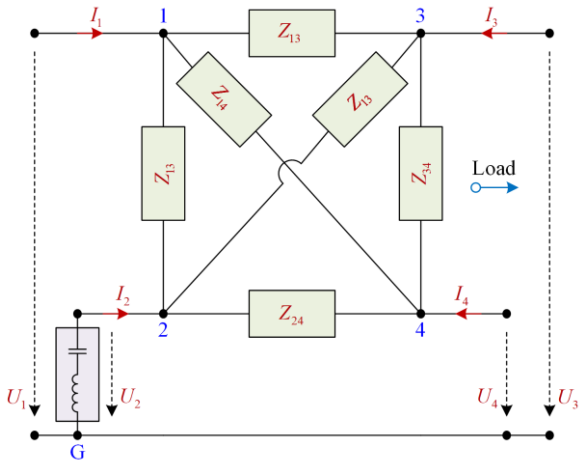

Fig. 5. Equivalent circuit of the transformer-filter combination.

Considering the impedance constraints of transformer winding, equation (8) and Fig. 4 can be simplified as (9) and Fig. 6.

$$\begin{cases}
Z_{12} = Z_{21} = Z_{k12} \\
Z_{23} = Z_{32} = \dfrac{Z_{k23}Z_{k24} - Z_{234}^2}{Z_{423}} \\
Z_{13} = Z_{31} = \infty \\
Z_{24} = Z_{42} = \dfrac{Z_{k23}Z_{k24} - Z_{234}^2}{Z_{324}} \\
Z_{14} = Z_{41} = \infty \\
Z_{34} = Z_{43} = \dfrac{Z_{k23}Z_{k24} - Z_{234}^2}{Z_{234}}
\end{cases} \tag{9}$$

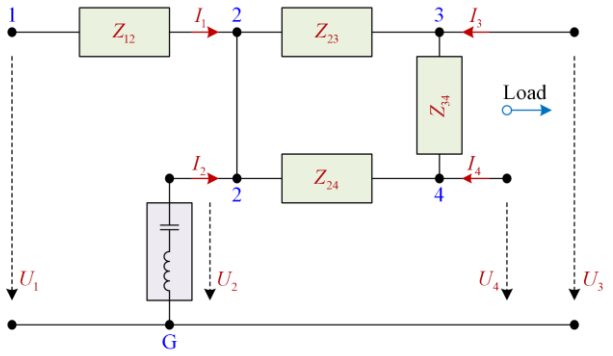

Fig. 6. Equivalent circuit considering the impedance constraints.

Figure 6 shows the simplified equivalent circuit with the consideration of impedance constraints. The direct connection between the primary winding (point 1) and load winding (points 3 or 4) is cut off. It can be summarized from the circuit model that:

1) For the harmonic current source from the power load, the flowing path turns to be 3→2→G or 4→2→G, which means that the harmonic components are isolated, and eliminated by the transformer-filter integrated system. Hardly any harmonics are existed at the primary side of the transformer.

2) For the harmonic voltage source from the power grid, its flowing path is blocked by the grid impedance and Z_{12}, as verified by (6), so that it almost has no impact on the power load, and the power quality of the power supply system is improved.

In conclusion, the transformer-filter integrated system owns excellent bi-directional harmonic-suppression ability, and realizes the harmonic isolation of upstream and downstream, so that the flowing path of harmonic is shortened. It is noted that the circuit model in Fig. 5 can be further simplified by means of Δ→Y conversion if necessary.

IV. Exploration & Optimization

This section mainly involves how to realize the zero-impedance design and the loss reduction in the permissible design range.

A. Impedance Calculation

As discussed in the previous section, the precondition of harmonic elimination includes the dual zero-impedance design of transformer winding, and it can be calculated by the short-circuit impedance as follows:

$$Z_{213} = (Z_{k12} + Z_{k23} - Z_{k13})/2 \tag{10}$$

$$Z_{214} = (Z_{k12} + Z_{k24} - Z_{k14})/2 \tag{11}$$

The short-circuit impedance between any two transformer windings is strongly associated with the structural parameters of the transformer. Figure 7 gives the winding structure. In Fig.7, r_0 is core radius; r_1, r_2, r_3 and r_4 are the center distance between core and winding; r_{34}, r_{42} and r_{21} are the center distance between core and air gap; a_1, a_2, a_3 and a_4 are the winding thickness; a_{03}, a_{34}, a_{42} and a_{21} are the insulation distance (air gap) between core and winding, or any two windings; h_x is the height of the transformer winding.

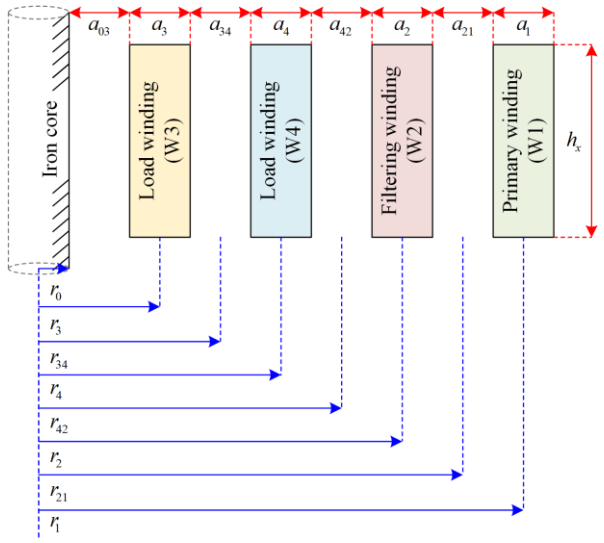

Fig. 7. Winding arrangement of the multi-winding transformer.

The above-mentioned center distances can be calculated by:

$$\begin{cases} r_3 = r_0 + a_{03} + a_3/2 \\ r_{34} = r_0 + a_{03} + a_3 + a_{34}/2 \\ r_4 = r_0 + a_{03} + a_3 + a_{34} + a_4/2 \\ r_{42} = r_0 + a_{03} + a_3 + a_{34} + a_4 + a_{42}/2 \\ r_2 = r_0 + a_{03} + a_3 + a_{34} + a_4 + a_{42} + a_2/2 \\ r_{21} = r_0 + a_{03} + a_3 + a_{34} + a_4 + a_{42} + a_2 + a_{21}/2 \\ r_1 = r_0 + a_{03} + a_3 + a_{34} + a_4 + a_{42} + a_2 + a_{21} + a_1/2 \end{cases} \tag{12}$$

Furthermore, the imaginary part of short-circuit impedance between any two windings can be obtained by [19]:

$$X_{kxy(\%)} = \frac{49.6 f \mu_0 NI \sum D_{xy} K \rho_{xy}}{H_{xy} e_t \times 10^6} \tag{13}$$

where f is the fundamental frequency; I and N are the rated current and turns of primary winding; μ_0 is absolute permeability, and $\mu_0 = 4\pi \times 10^{-7}$ H/m; ρ_{xy} is the Rogowski coefficient between W_x and W_y; K is additional reactance coefficient; $\sum D_{xy}$ is the magnetic flux leakage area between W_x and W_y; e_t is the electric potential of each turn; H_{xy} is arithmetic mean height of W_x and W_y.

Rogowski coefficient is closely related to the structural parameters, which can be calculated by:

$$\begin{cases} \rho_{12} = 1 - \dfrac{a_2 + a_{21} + a_1}{\pi H_{12}} \\ \rho_{14} = 1 - \dfrac{a_4 + a_{42} + a_2 + a_{21} + a_1}{\pi H_{14}} \\ \rho_{24} = 1 - \dfrac{a_4 + a_{42} + a_2}{\pi H_{24}} \\ \rho_{23} = 1 - \dfrac{a_3 + a_{34} + a_4 + a_{42} + a_2}{\pi H_{23}} \\ \rho_{13} = 1 - \dfrac{a_3 + a_{34} + a_4 + a_{42} + a_2 + a_{21} + a_1}{\pi H_{13}} \end{cases} \tag{14}$$

The expression of magnetic flux leakage area used in (13) is:

$$\begin{cases} \sum D_{12} = \dfrac{1}{3}(a_2 r_2 + a_1 r_1) + a_{21} r_{21} \\ \sum D_{13} = \dfrac{1}{3}(a_3 r_3 + a_1 r_1) + (a_{34} + a_4 + a_{42} + a_2 + a_{21}) \times \\ \qquad (r_3 + \dfrac{a_3 + a_{34} + a_4 + a_{42} + a_2 + a_{21}}{2}) \\ \sum D_{14} = \dfrac{1}{3}(a_4 r_4 + a_1 r_1) + (a_{42} + a_2 + a_{21}) \times \\ \qquad (r_4 + \dfrac{a_4 + a_{42} + a_2 + a_{21}}{2}) \\ \sum D_{23} = \dfrac{1}{3}(a_2 r_2 + a_3 r_3) + (a_{34} + a_4 + a_{42}) \times \\ \qquad (r_3 + \dfrac{a_3 + a_{34} + a_4 + a_{42}}{2}) \\ \sum D_{24} = \dfrac{1}{3}(a_2 r_2 + a_4 r_4) + a_{42} r_{42} \end{cases} \tag{15}$$

At this point, the equations used for the impedance calculation are all deduced in (10)–(15). The precondition of impedance matching can be easily reached by means of proper design of the transformer. In other word, once the main design parameters (rated capacity

or rated voltage) of the transformer are determined, the air gap becomes the only adjustable variable, as the structural parameters listed in Table II. Inspired by this, a low-loss improvement method is developed under the constraints of dual zero-impedance.

TABLE II
STRUCTURAL PARAMETERS OF TRANSFORMER

Item	Value	Item	Value
r_0	45 mm	a_{42}	※
a_{03}	5 mm	a_2	23 mm
a_3	6.5 mm	a_{21}	※
a_{34}	※	a_1	8 mm
a_4	6.5 mm	e_r	100/$\sqrt{3}$ /32 V
h_1	172 mm	h_2	170 mm
h_3	170 mm	h_4	173 mm

Note: ※ indicates the variable.

B. Design Margin

Figure 8 shows the surface of dual zero-impedance (i.e., equations (10) and (11)), which uses the distances of air gap as the variables (a_{34}-a_{42}-a_{21}). The upper surface is X_{214}, and the lower one is X_{213}. The variation range for the distances of air gap is [0, 60 mm], while it seems large for a practical transformer (a wide air gap results in the increase of materials and costs); however, it is convenient for us to observe the trend of the two surfaces. It can be clearly found that there is no crossing line between the two surfaces, which means that it is hardly to realize dual absolute zero-impedance in the wide range. To solve this issue, the approximative impedance design is presented here. The definitions are given as follows:

1) Absolute zero-impedance: it is strictly satisfied that $X_{213}=0.0\%$ and $X_{214}=0.0\%$. The design margin is shown in Fig. 8.

2) Approximative zero-impedance: the equivalent impedances of X_{213} and X_{214} are allowed within a small range, so that the crossing region can be created. The variation in the small range will not affect the filtering performance. The design margins are shown in Figs. 9–10.

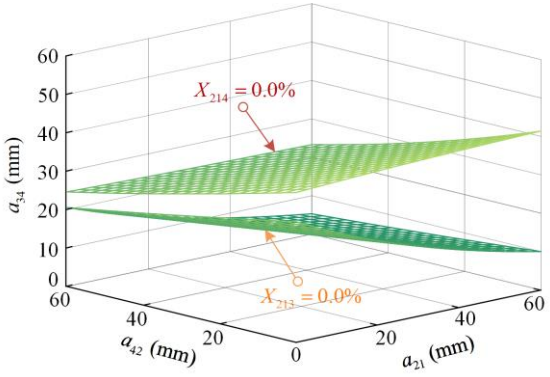

Fig. 8. Surfaces of dual absolute zero-impedance.

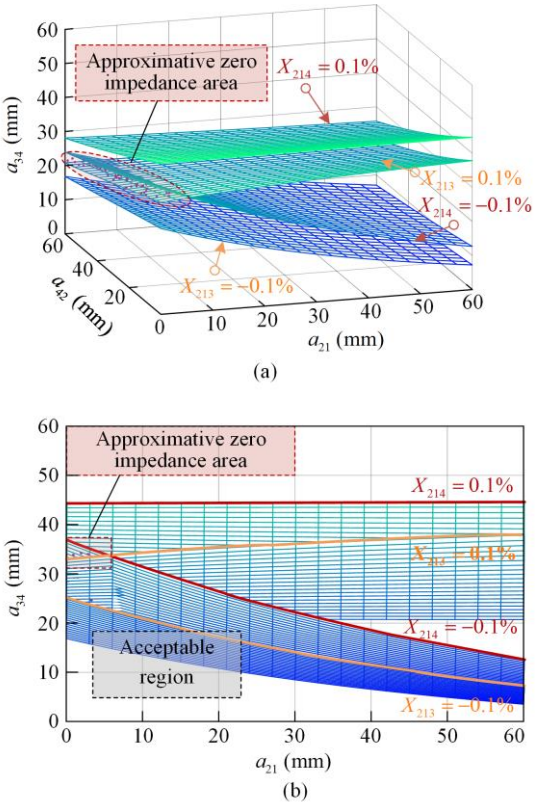

Fig. 9. Surface of dual approximative zero-impedance area with range [−0.1%, 0.1%]. (a) Space using a_{34}-a_{42}-a_{21} as variables. (b) Plane using a_{34}-a_{21} as variables.

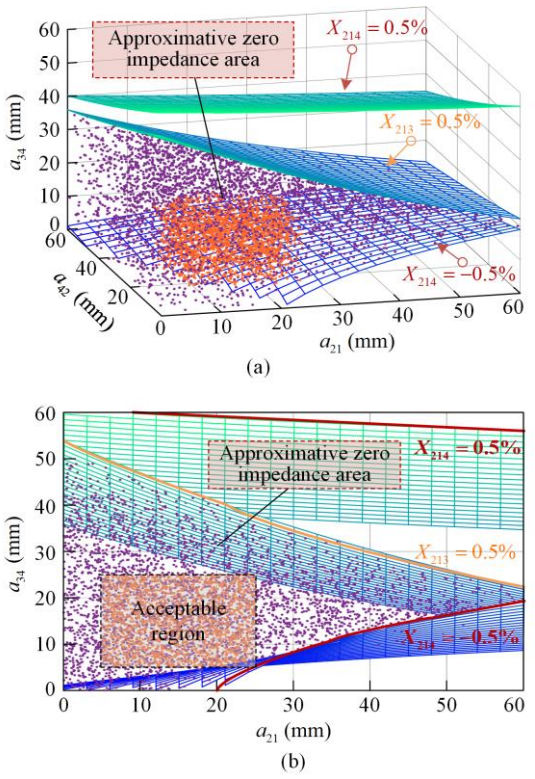

Fig. 10. Surface of dual approximative zero-impedance area with range [−0.5%, 0.5%]. (a) Space using a_{34}-a_{42}-a_{21} as variables. (b) Plane using a_{34}-a_{21} as variables.

Figure 9 gives an example of approximative zero-impedance. The variation range is set as [−0.1%, 0.1%]. The purple dots that meet the approximative zero-impedance are generated by means of Monte Carlo method in Fig. 9(a). It is shown that all the feasible points are located in the region surrounded by upper surface ($X_{214}=-0.1\%$) and lower surface ($X_{213}=0.1\%$). The acceptable region for the distances of air gap is defined as [5 mm, 25 mm], which is marked in Fig. 9(b). However, no feasible point exists in the acceptable region in this case.

Given this, the variation range of approximative zero-impedance is enlarged in Fig. 10. Orange dots represent the feasible point in the acceptable region of air gap. The acceptable region is a cube sectioned by the lower surface ($X_{214}=-0.5\%$). The transformer optimization will be explored in the range of acceptable structural parameter.

C. Optimization

The derivation process of the transformer loss and efficiency is given in Appendix A. The optimization objective is to maximize the transformer efficiency, with optimization strategy shown as (16). It is noted that the acceptable region is set in [5mm, 25mm], the same as mentioned before.

The optimization result is shown in Fig. 11, in which load factor β is used as variable with the step size of 0.1. Specifically, the corresponding parameters (structural parameter, equivalent impedance and efficiency) are also listed in Table III. It can be concluded from the results that:

1) With the extension of impedance constraint domain, the transformer efficiency is also increased, while the filtering performance is slightly degraded inevitably;

2) Due to the restriction of structural parameters, there is little difference of optimization results between Case 3 and Case 4;

3) Compared with Case 1, the efficiency of Case 4 is improved by 0.5% ($\beta=0.3$).

In sum, there must be a trade off to balance filtering performance and transformer efficiency.

$$\begin{cases} \text{obj. } \max\{\eta(a_{34},a_{42},a_{21})\} \\ \text{s.t.} \begin{cases} \text{Case 1:} -0.2 \leqslant X_{213} \leqslant 0.2 \ \& -0.2 \leqslant X_{214} \leqslant 0.2 \\ \text{Case 2:} -0.3 \leqslant X_{213} \leqslant 0.3 \ \& -0.3 \leqslant X_{214} \leqslant 0.3 \\ \text{Case 3:} -0.4 \leqslant X_{213} \leqslant 0.4 \ \& -0.4 \leqslant X_{214} \leqslant 0.4 \\ \text{Case 4:} -0.5 \leqslant X_{213} \leqslant 0.5 \ \& -0.5 \leqslant X_{214} \leqslant 0.5 \\ a_{\min} \leqslant a_{34} \leqslant a_{\max} \\ a_{\min} \leqslant a_{42} \leqslant a_{\max} \\ a_{\min} \leqslant a_{21} \leqslant a_{\max} \end{cases} \end{cases} \tag{16}$$

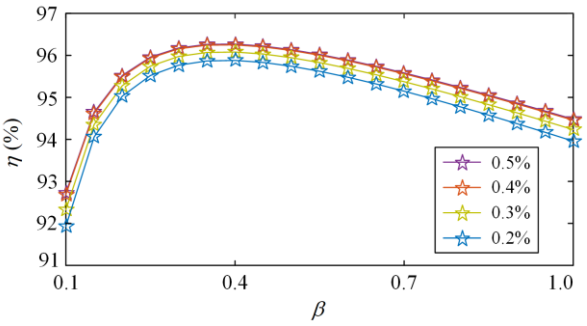

Fig. 11. Optimized efficiency.

TABLE III
OPTIMIZATION RESULTS

Case	a_{34} (mm)	a_{42} (mm)	a_{21} (mm)	X_{213} (%)	X_{214} (%)	η (%) ($\beta=0.3$)	η (%) ($\beta=0.5$)	η (%) ($\beta=0.7$)	η (%) ($\beta=0.9$)
1	5.00	10.67	25.00	−0.0360	−0.2000	95.77	95.74	95.15	94.38
2	5.00	5.00	17.87	−0.1697	−0.3000	95.98	95.95	95.37	94.63
3	5.00	5.00	6.29	−0.3163	−0.4000	96.16	96.12	95.56	94.84
4	5.00	5.00	5.00	−0.3296	−0.4082	96.27	96.14	95.58	94.87

V. VERIFICATION TEST

A down-scaled experimental platform of the industrial power supply system based on the transformer prototype is established. The transformer prototype is produced according to the parameters of Case 3, whose picture is shown in Fig. 12. Simulation validation for different cases, and experimental tests for filtering performance and transformer loss are all designed to verify the theoretical analysis. Tables IV gives the related parameters of the prototype.

Fig. 12. Transformer prototype.

TABLE IV
DESIGN PARAMETERS OF TRANSFORMER

Parameter	Primary winding (W1)	Filtering winding (W2)	Load winding (W3)	Load winding (W4)
Wiring scheme	Y	Δ	Y	Δ
Rated voltage (V)	220	220	$100/\sqrt{3}$	100
Rated capacity (kVA)	20	10	10	10
Number of turns	122	122	32	55
Equivalent impedance (%)	X_{213}		−0.31%	
	X_{214}		−0.40%	

A. Simulation: Verification of Cases

Given the difficulty to test the Cases 1–4 in Table III by experiment, the relevant verification is made by simulation, with the results shown in Table V. Case 5 indicates the inductive filtering transformer without structural optimization method, and Case 6 refers to the implementation of Case 3 at the condition of open circuit of the filtering winding, while Case 7 is the conventional three winding transformer without inductive filtering method and structural optimization method. The basic parameters of Cases 5 and 7, e.g., rated voltage and rated capacity, are the same with Cases 1–4. THD_I in the table refers to the total harmonic distortion of current. For Cases 1–4, as the improvement of efficiency, the filtering performance gets relatively poor. Case 3 is hence selected as acceptable reference for prototype to balance performance and efficiency. More details can be found that the harmonic suppression at the secondary side also leads to loss reduction as analyzed in Section III (Cases 5 and 7), while the structural optimization method can contribute to further efficiency improvement (Cases 5 and 3). It is noted that from Case 3 and Cases 6–7 that, although the filter is not implemented (Case 6), the transformer efficiency is still increased compared with Case 7, due to the efficiency optimization. Moreover, the increase of power factor (PF) is conducive to loss reduction (Case 7 and Cases 1–5). For no-load loss, it changes little under different cases, which shows that the optimization of no-load loss accounts for a small proportion in the total loss.

TABLE V
SIMULATION RESULTS

Case	η (%) ($\beta = 0.3$)	THD (%) (Current)	PF
1	95.82	2.99	0.996
2	96.10	3.24	0.996
3 (Adopted)	96.33	3.89	0.995
4	96.45	3.96	0.995
5	95.65	3.40	0.995
6	95.70	9.51	0.973
7	95.23	9.55	0.973

B. Experiment 1: Harmonic Suppression Test

The harmonic suppression ability of the proposed transformer-filter combination is tested. Figure 13 is the current waveforms of the prototype recorded at primary side, load side (W3) and load side (W4) respectively. It can be found that, with the help of the phase-shift structure (30° phase difference of the currents between the two load sides) and the inductive filtering method, the current quality at the primary side is greatly improved. THD_I is dropped from 27.73% (load side) to 4.34% (primary side).

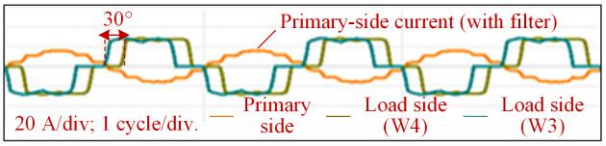

Fig. 13. Experimental waveform at different test point of the prototype.

Figure 14 shows the comparison test results for Case 3 and Case 7. Table VI lists the harmonic content corresponding to the waveforms in Fig. 14. Although most of the harmonic components are offset due to the 12-pulse structure, $12k \pm 1$ order harmonic current still exists in the primary-side current ($k = 1, 2, 3...$), which experimentally results in the THD of 10.00% for Case 7. Compared with the conventional structure, the harmonic suppression ability of Case 3 gets better. However, its performance is still inevitably influenced by the approximative zero-impedance design. The filtering rates for the tuned frequency harmonics are 69.32% (550 Hz) and 61.53% (650 Hz).

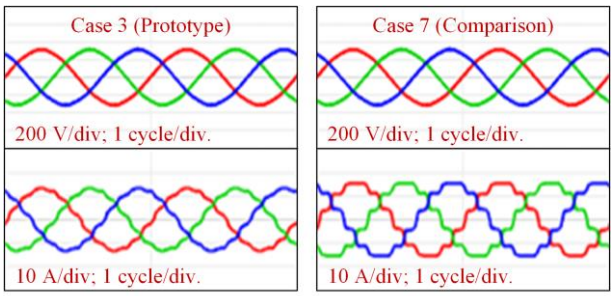

Fig. 14. Primary-side current and voltage waveforms. (a) Case 3 for prototype. (b) Case 7 for comparison.

TABLE VI
EXPERIMENTAL RESULTS

Harmonic order	Primary-side current (A) (Case 3)	Primary-side current (A) (Case 7)	Load-side current (A) (W3)	Load-side current (A) (W4)
Fun.	11.05	11.02	21.07	20.73
5	0.12	0.15	4.44	4.63
7	0.12	0.13	2.52	2.13
11	0.27	0.88	1.68	1.56
13	0.25	0.65	1.25	1.12
17	0.06	0.05	0.89	0.80
19	0.04	0.04	0.70	0.61

C. Experiment 2: Efficiency Improvement Test

The zero-impedance deviation brings about the efficiency improvement of rectifier transformer. Figure 15 is the efficiency test results under different load factors. The comparison is made between Case 3 and Cases 6–7. Case 6, as a special condition of Case 3, shows a satisfactory improvement of transformer efficiency even under harmonic environment, which can be attributed to the low loss design in Section IV. With the implementation of inductive filtering method, the efficiency of Case 3 can reach 96.10% under light load, while the average improvement can be 0.79% compared with Case 7. However, the test results are a little lower than that of theoretical analysis and simulation value, which can be attributed to the nonnegligible internal resistance in the low power experimental system.

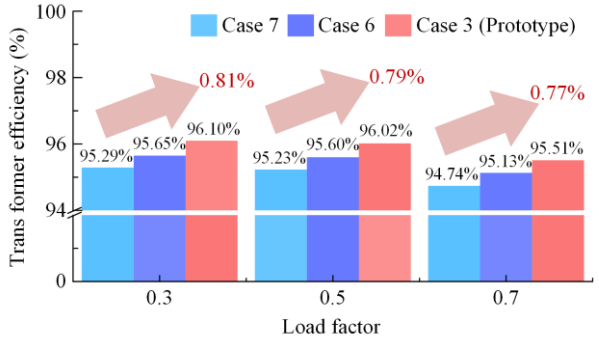

Fig. 15. Efficiency improvement test result.

VI. Conclusion

A novel transformer winding design strategy is presented, and the corresponding industrial power supply system is further developed in this article, which shows strong ability in harmonic suppression and efficiency improvement in the high-current application. The contributions and findings, i.e., the answers for the questions mentioned in Introduction, are summarized as follows.

1) What is the filtering principle of the special transformer-filter combination?

By means of modelling of the combination, it can be concluded that the harmonic components can be offset inside the transformer, so that the harmonic magnetic potential self-balance between the secondary windings is realized.

2) How to get the precondition of low-loss design for the multi-winding transformer?

It is found from the expression of primary-side current that, it is necessary precondition that the equivalent impedances $Z_{213}=0$ and $Z_{214}=0$, which is different from the common three-winding transformer.

3) How to determine the design margin of the transformer?

To get the design margin, the concept of limited approximative zero-impedance is proposed, which still promises satisfactory performance. The feasible structural parameters are also determined within the design margin.

4) Considering the constraint of precondition, how to realize the efficiency improvement?

The optimal efficiency is searched and determined in the interval of design margin. The efficiency is verified experimentally to be improved by 0.81% under light load.

Appendix A

Figure A1 shows the proposed transformer structure included the iron core, where A_z and A_e are the sectional area of iron yoke and core limb; h_0 and h_e are the height of iron yoke and core limb window; M_0 is the center distance of core limb; a_p is the air gap between the windings of each phase. There is following relationship between M_0 and a_p.

$$M_0 = 2\times[r_1+(a_1+a_p)/2] \tag{A1}$$

where a_p is a fixed quantity, and $a_p = 10$ mm.

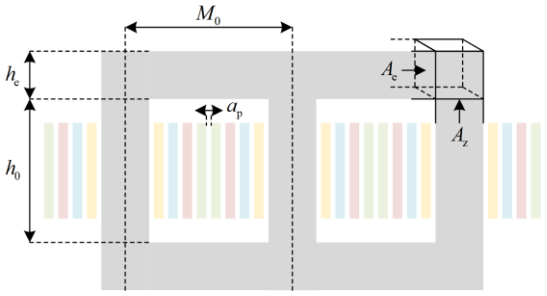

Fig. A1. Transformer structure.

A. No-load Loss

The no-load loss can be calculated as follows:

$$\begin{cases} P_0 = K_p P_c (G_1+G_2+G_3) \\ G_1 = 2A_z h_e \gamma_{Fe} \\ G_2 = 4A_e M_0 \gamma_{Fe} \\ G_3 = 3A_z h_0 \gamma_{Fe} \end{cases} \tag{A2}$$

where K_p is the coefficient related to the core material, and $K_p = 1.3$; P_c is the specific loss related to the flux density of iron yoke and core limb, and $P_c = 0.8$ W/kg; G_1, G_2 and G_3 are the corner weight, yoke weight and limb weight; γ_{Fe} is the density of silicon steel, $\gamma_{Fe} = 7.65$ kg/cm^3.

B. Load Loss

The length l_x and resistance R_x of the transformer winding are deduced as,

$$l_x = 2\pi r_x N_x \tag{A3}$$

$$R_x = \rho l_x / A_x \tag{A4}$$

where N_x is the corresponding winding turn; A_x is the sectional area of single coil ($x=1, 2, 3, 4$); ρ is the resistivity of copper wire at 75℃, and $\rho = 0.02097\ \Omega \cdot \text{mm}^2/\text{m}$.

The resistive loss of the transformer is obtained as:

$$P_{\text{k}} = 1.05\sum_{i=1}^{4} 3I_i^2 R_i \tag{A5}$$

where the coefficient 1.05 is to include the additional loss and stray loss.

C. Transformer Efficiency

It can be concluded from the deduction that, all the loss related formulas include the distance of air gap (a_{34}, a_{42} and a_{21}). In other word, we can obtain the loss equations using the distance of air gap as variable, i.e., $P_0(a_{34}, a_{42}, a_{21})$ and $P_{\text{k}}(a_{34}, a_{42}, a_{21})$. Furthermore, the transformer efficiency is also defined as follows.

$$\eta(a_{34}, a_{42}, a_{21}) = \left(1 - \frac{P_0 + \beta^2 P_{\text{k}}}{S_{\text{N}}\beta\cos\varphi + P_0 + \beta^2 P_{\text{k}}}\right) \times 100\% \tag{A6}$$

where S_{N} is the rated capacity; β is load factor; $\cos\varphi$ is the load power factor, and $\cos\varphi$ is set as 0.9.

ACKNOWLEDGMENT

Not applicable.

AUTHORS' CONTRIBUTIONS

Qianyi Liu: background research, theoretical analysis, simulation validations, experiment validations, full-text writing and the construction of the paper framework. Fang Liu: supervision and manuscript review & editing. Yi Yang: software and simulations. Yanjian Peng: supervision and manuscript review. Kang-Zhi Liu: supervision and manuscript review. Ao Wang: manuscript review. All authors read and approved the final manuscript.

FUNDING

This work is supported in part by the National Natural Science Foundation of China (No. 52207146), in part by the Jiangsu Province Engineering Research Center of High-Level Energy and Power Equipment (No. JSNYDL-202401), in part by the Science and Technology Innovation Program of Hunan Province (No. 2023GK2007), in part by the Natural Science Foundation of Hunan Province of China (No. 2024JJ3033), and in part by the National Natural Science Foundation of China (No. 62373373).

AVAILABILITY OF DATA AND MATERIALS

Not applicable.

DECLARATIONS

Competing interests: The authors declare that they have no known competing financial interests or personal relationships that could have appeared to influence the work reported in this article.

AUTHORS' INFORMATION

Qianyi Liu was born in Sichuan, China, in 1992. He received the B.Sc. degree in electrical engineering and its automation (railway electrification) from the Department of Electrical Engineering, Southwest Jiaotong University, Chengdu, China, in 2014, and the M.Eng. and Ph.D. degrees in electrical engineering from the College of Electrical and Information Engineering, Hunan University, Changsha, China, in 2017 and 2020, respectively. From 2019 to 2020, he was a visiting Ph.D. student with the Institute of Energy Systems, Energy Efficiency, and Energy Economics, TU Dortmund University, Dortmund, Germany. Since 2021, he has been a lecturer of electrical engineering with the School of Automation, Central South University, Changsha, China. His research interests include electric power optimization and control.

Fang Liu was born in Jiangxi, China, in 1982. She received the B.S. degree from the College of Electric and Information Engineering, Zhengzhou University of Light Industry, Zhengzhou, China, in 2005, and the Ph.D. degree from Waseda University, Tokyo, Japan in 2011. Since 2017, she has been a professor with the School of Automation, Central South University, Changsha, China. Her main research interests include stability analysis of time-delay system and power system, and robust control of FACTS with wide-area signals.

Yi Yang received the B.Eng. degree in electrical engineering and its automation and the M.Eng. degree in control theory and control engineering from Central South University, Changsha, China, in 2021 and 2024, Her research interests include electric power optimization.

Yanjian Peng received the B.S. degree in electrical engineering from University of Jinan, Shandong, and the Ph.D. degree in electrical engineering from Hunan University, Hunan, China, in 2011, and 2021, respectively. He is currently a postdoctoral fellow with the College of Electrical and Information Engineering, Hunan University, Hunan, China. His research interests include power quality analysis, and grid connected applications based on voltage source converter for wind turbine applications.

Kang-Zhi Liu received the B.E. degree in control engineering from Northwestern Polytechnical University, Xi'an, China, in 1984, and the M.E. and Ph.D. degrees in electrical engineering from Chiba University, Chiba, Japan, in 1991 and 1998, respectively. Since then, he has been with Chiba University, where he is currently a professor. He has authored and coauthored six books. His research interests include control theory, power systems, smart grids, and machine learning. Dr. Liu was the recipient of the Young Author Award and three Best Paper Awards from SICE, Japan. He was the director of SICE in 2017, 2018, and was elected as a fellow of SICE in 2022.

Ao WANG was born in Jiangsu, China in 1991. He holds a Ph.D. degree and serves as a master's supervisor. He graduated from Nanjing University of Science and Technology in 2021 with a major in engineering thermophysics, under the guidance of professor Yimin Xuan, a renowned engineering thermophysicist and academician of the Chinese Academy of Sciences. Presently, he is employed at the School of Mechanical and Rail Transit Engineering, Changzhou University, where he conducts research related to solar energy conversion and utilization, new energy, and the development of energy-saving and environmental protection equipment. He has presided over and participated in 8 national, provincial, and municipal projects, and published 13 academic papers.

REFERENCES

[1] Q. Du, L. Gao, and Q. Li *et al*., "Harmonic reduction methods at DC side of parallel-connected multipulse rectifiers: a review," *IEEE Transactions on Power Electronics*, vol. 36, no. 3, pp. 2768-2782, Mar. 2021.

[2] H. Tao, C. Zhang, and M. Zhao *et al*., "Harmonic analysis and hybrid control of a cascaded H-bridge rectifier," *Power System Protection and Control*, vol. 51, no. 22, pp. 24-33, Nov. 2023. (in Chinese)

[3] R. Fuentes, J. Estrada, and L. Neira *et al*., "Increasing copper production in electrochemical plants using new small transformer-rectifiers in parallel with existing power rectifiers," *IEEE Transactions on Industry Applications*, vol. 52, no. 1, pp. 641-644, Jan. 2016.

[4] J. R. Rodriguez, J. Pontt, and C. Silva *et al*., "Large current rectifiers: state of the art and future trends," *IEEE Transactions on Industrial Electronics*, vol. 52, no. 3, pp. 738-746, Jun. 2005.

[5] J. Lai, X. Yin, and X. Yin *et al*., "Typology and working mechanism of a hybrid power router based on power-frequency transformer electromagnetic coupling with converters," *Protection and Control of Modern Power Systems*, vol. 8, no. 3, pp. 1-17, Jul. 2023.

[6] W. Wang, A. Nysveen, and N. Magnusson, "Eddy current loss in grain-oriented steel laminations due to normal leakage flux," *IEEE Transactions on Magnetics*, vol. 57, no. 6, pp. 1-4, Jun. 2021.

[7] T. Dao, B. T. Phung, and T. Blackburn, "Effects of voltage harmonics on distribution transformer losses," in *2015 IEEE PES Asia-Pacific Power and Energy Engineering Conference*, Brisbane, Australia, Nov. 2015, pp. 1-5.

[8] D. Yildirim and E. F. Fuchs, "Measured transformer derating and comparison with harmonic loss factor (F/sub HL/) approach," *IEEE Transactions on Power Delivery*, vol. 15, no. 1, pp. 186-191, Jun. 2000.

[9] IEEE Recommended Practice for Establishing Liquid-Filled and Dry-Type Power and Distribution Transformer Capability When Supplying Nonsinusoidal Load Currents, IEEE Std C57.110-2008 (Revision of IEEE Std C57.110-1998), 2008.

[10] L. Peretto, R. Sasdelli, and G. Serra, "Measurement of harmonic losses in transformers supplying nonsinusoidal load currents," *IEEE Transactions on Instrumentation and Measurement*, vol. 49, no. 2, pp. 315-319, Apr. 2000.

[11] N. Kurita, A. Nishimizu, and C. Kobayashi *et al*., "Magnetic properties of simultaneously excited amorphous and silicon steel hybrid cores for higher efficiency distribution transformers," *IEEE Transactions on Magnetics*, vol. 54, no. 11, pp. 1-4, Nov. 2018.

[12] S. Takajo, T. Ito, and T. Omura *et al*., "Loss and noise analysis of transformer comprising grooved grain-oriented silicon steel," *IEEE Transactions on Magnetics*, vol. 53, no. 9, pp. 1-6, Sept. 2017.

[13] T. Ding and W. Xu, "A filtering scheme to reduce the penetration of harmonics into transmission systems," *IEEE Transactions on Power Delivery*, vol. 31 no. 1, pp. 59-66, Feb. 2016.

[14] E. Lei, X. Yin, and Z. Zhang *et al*., "An improved transformer winding tap injection DSTATCOM topology for medium-voltage reactive power compensation," *IEEE Transactions on Power Electronics*, vol. 33, no. 3, pp. 2113-2126, Mar. 2018.

[15] T. Wang, F. Fang, and X. Jiang *et al*., "Performance and design analysis on round-shaped transformers applied in rectifier systems," *IEEE Transactions on Industrial Electronics*, vol. 64, no. 2, pp. 948-955, Feb. 2017.

[16] S. R. Mousavi-Aghdam, "A new design and analysis of round-shaped transformers supplying diode and controllable rectifiers," *IEEE Transactions on Industrial Electronics*, vol. 66, no. 11, pp. 8394-8401, Nov. 2019.

[17] Y. Li, L. Luo, and C. Rehtanz *et al*., "An industrial DC power supply system based on an inductive filtering method," *IEEE Transactions on Industrial Electronics*, vol. 59, no. 2, pp. 714-722, Feb. 2012.

[18] Y. Tian, L. Luo, and Q. Liu *et al*., "A new harmonic mitigation system with double balanced impedance filtering power transformer for multistage distribution network," *IEEE Transactions on Industrial Electronics*, vol. 68, no. 6, pp. 4565-4575, Jun. 2021.

[19] B. An, Y. Li, and X. Hua *et al*., "Magnetic-integrated multipulse rectifier transformer with a tight impedance equalizing strategy for power quality improvement of DC traction power supply system," *IEEE Transactions on Industrial Electronics*, vol. 67, no. 8, pp. 6270-6279, Aug. 2020.